WORLD CONFERENCE ON TIMBER ENGINEERING 2025
BRISBANE, AUSTRALIA
Advancing Timber for the Future Built Environment

PROPAGATION IN WOOD OF A CRACK DEVIATED FROM THE DIRECTION OF THE FIBERS

Nouradine HASSAN IBRAHIM[1], Rostand MOUTOU PITTI[1,2], Nicolas SAUVAT[1], Benoit BLAYSAT[1], Joseph GRIL[1], Arthur Bontemps[3], Thomas JAILIN[1]

ABSTRACT: This work focuses on conducting fracture tests on wood, particularly silver fir (*Abies alba*), to track crack propagation using imaging-based methods and to examine the influence of fiber orientation on this phenomenon. Specimens of the Mixed Mode Crack Growth (MMCG) and Tapered Double Cantilever Beam (TDCB) types with different fiber orientations were studied to evaluate the energy release rate using the imposed displacement method in opening mode. Then, the energy release rate G was calculated on both faces of the specimens to evaluate the influence of the observed face. Finally, a scanning electron microscope (SEM) was used to observe local cracking processes, and determine whether the bifurcation of the crack is induced by a mechanical effect or by the oriented fibrous structure of the material. This study deepens our understanding of the mechanisms of crack propagation in wood and the influence of fiber orientation, by combining experimental tests, numerical simulations, and microscopic observations.

KEYWORDS: Crack, Silver fir, fiber orientation, LSA, SEM

1 – INTRODUCTION

The environmental challenges facing our planet have heightened the need to adopt materials that contribute to carbon sinks, in accordance with the recommendations of COP28-29 **[1]**. Wood stands out as one of the few natural materials that meet these ecological criteria, thanks to its ability to sequester carbon throughout its lifecycle. Indeed, wood is a composite material made of natural polymers ; it constitutes the most significant renewable raw material in terms of volume. Its recyclability and biodegradability make it a material of great interest. From an environmental perspective, it can store carbon dioxide, which is considered one of the main greenhouse gases.

Wood is also one of the most widely used materials in civil construction, where structural elements benefit from its excellent mechanical performance and unique properties. It is impact-resistant, lightweight, stable, and durable, as demonstrated by Asian temples built from wood that have withstood over more than ten centuries **[2]**.

To better understand the deformation and failure mechanisms of wood under prolonged loading, bending creep tests on notched beams were conducted during Arthur Bontemps' PhD research **[3]**. These tests revealed a deviation in crack direction relative to the alignment of the wood fibers. This deviation was interpreted as a systematic adjustment of the crack propagation path, exploiting the wood's anatomical structure.

To verify this hypothesis, an experimental study was conducted on the influence of fiber orientation on crack propagation and the measurement of the energy release rate. A contactless field measurement method, the Localized Spectral Analysis (LSA), was used to observe crack propagation in fir (*Abies alba*) beams, along with measurements of fibre and crack slopes. It was used to estimate the elastic energy release rate resulting from the propagation of the crack. Observations of the anatomical structures were then conducted using a scanning electron microscope (SEM) to explain the observed crack propagation behavior.

2 – METHOD

In this section, we explore the opening mode fracture behaviour of silver fir using the LSA method. The geometries of the MMCG and variable inertia Cantilever specimens are presented. The detail regarding the design of the specimens are provided in the following section.

2.1 SPECIMENS

Two geometries were tested in this study. The TDCB (Tapered Double Cantilever Beam) specimen (Fig. 1a)

[1] Nouradine Hassan Ibrahim, Rostand Moutou Pitti, Nicolas Sauvat, Joseph Gril, Thomas Jalin, Benoît Blaysat, Université Clermont Auvergne, CNRS, Clermont Auvergne INP, Institut Pascal, 63000 Clermont-Ferrand, France

[2] Rostand Moutou Pitti, CENAREST, IRT, BP 14070, Libreville, Gabon, rostand.moutou_pitti@uca.fr

[3] Arthur Bontemps, Université de Lyon, ECAM LaSalle, 69005 Lyon, France

https://doi.org/10.52202/080513-0203

provides a good range of stable crack propagation **[4]**. This geometry has been chosen for its ease of fabrication and its suitability for Mode I fracture tests. A second geometry was also used, the MMCG specimen developed by MOUTOU PITTI **[5]** , which allows stable crack propagation after its initiation (Figure 1b).

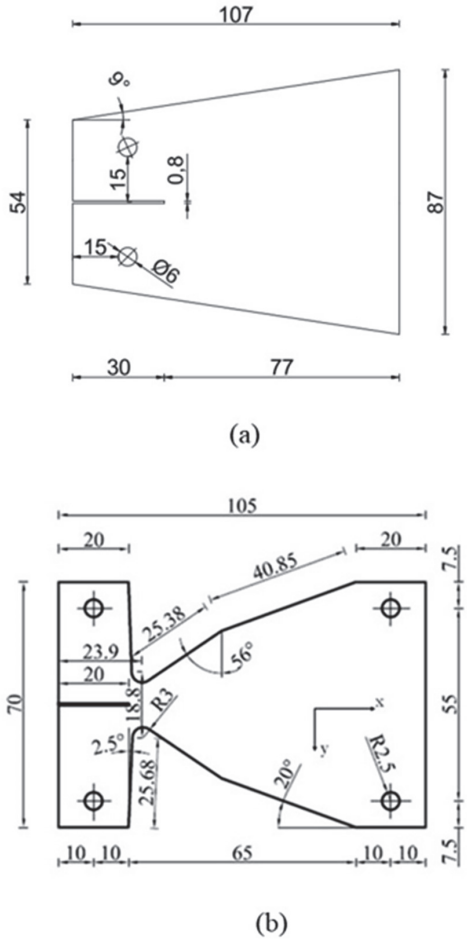

Figure 1 : Geometry of specimens (a) TDCB; (b) MMCG

Samples were cut in almost the RL direction. The angle between the radial direction and cut is between 30 and 45°.

Nine TDCB and MMCG specimens were identified and classified for these beams based on the angle between cut and fiber angle (Figure 2).

The cantilever specimens were sawn, while the MMCG specimens were laser-cut to ensure that each specimen conforms to the desired dimensions.

The notation used for specimens is as follows:

- **T0-a: T** (TDCB); **0** (0° Fiber angle); **a** (First specimen of this type)
- **M23-b:M** (MMCG); **23** (23° Fiber angle); **b** (Second specimen of this type)

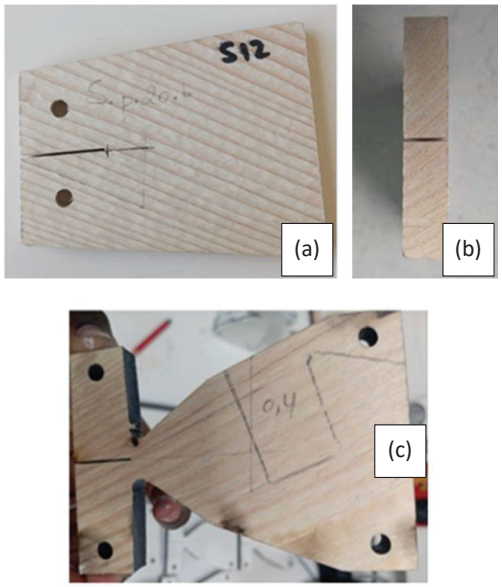

Figure 2 : (a) Face of specimen T7-a; (b) and edge ; (c) Specimen M23-a

2.2 ENERGY RELEASE RATE G

Griffith's energy G is defined as the variation of energy per unit of the cracked surface when a crack propagates in a linear elastic material. Crack propagation occurs when Griffith's energy reaches a critical value, denoted as Gc. This critical value Gc corresponds to a measure of the material's toughness.

In Griffith's initial theory, which applies to brittle fracture, the energy ΔU corresponds to the energy required to create new surfaces in the material. Griffith's energy G is expressed per unit surface and is defined from ΔU as follows:

$$G = \lim_{\Delta A \to 0} \frac{\Delta U}{\Delta A} = \frac{\partial U}{\partial A}, \qquad (1)$$

where ΔA = b x Δa, is the cracked surface during crack propagation over the length Δa in a specimen with a thickness b. Generally, b = 1 is considered as a unit thickness, Υ_s representing the specific surface energy. Thus, G is given by the following expression:

$$G = \frac{\partial U}{\partial A} = 2\Upsilon_s \qquad (2)$$

In the case of imposed displacement and when the thickness b is not equal to unity, the final expression for the energy restitution rate is:

$$G_c = \frac{F_{ci}^2}{2b} \times \left(\frac{\partial C}{\partial a}\right)_d \qquad (3)$$

https://doi.org/10.52202/080513-0203

F_{ci} (i = 1,2,3…) is the so-called critical force, which indicates an increase Δa in the length of the crack a. Compliance is defined by $\Delta C = \frac{U_i}{F_{ci}}$ that U_i the crack opening induced by each critical force F_{ci} . In the relationship G_c , ΔC is the increase in compliance corresponding to the observed increase in crack length by an amount Δa. The subscript "$_d$" indicates that the test is performed with an imposed displacement.

2.3 LOCALIZED SPECTRAL ANALYSIS METHOD

Localized Spectrum Analysis (LSA) is a technique based on the windowed Fourier transform (WFT) for analyzing periodic patterns in images. This method is particularly effective for extracting displacement and strain fields with high precision while minimizing noise inherent in camera sensors [6].

This innovative spectral technique minimizes the optical residue in the Fourier domain, significantly reducing the computational cost of displacements. It is particularly effective for processing images of checkerboard patterns and other periodic patterns, such as two-dimensional grids [7].

To apply LSA, a checkerboard pattern must be engraved onto the surface of the specimen being studied. Two layers of white paint must be applied to prepare this surface. In our tests, we used Spartex RAL 9010 white paint to achieve a uniform and contrasted surface. After painting, a laser-equipped engraving machine creates the precise checkerboard pattern on the specimen.

On each specimen, two checkerboard patterns were marked (figure 4) : a small checkerboard of 30 µm on the first face and a large checkerboard of 70 µm on the second.

Procedure 2 of the LSA described in [6] is an accurate method for analyzing deformations in two perpendicular directions using checkerboard patterns transformed into 1D grids.

The checkerboard pattern is then transformed into two perpendicular 1D grids, one in the X direction and the other in the Y direction. The windowed Fourier transform (WFT) is applied to each of these grids to convert from image space to the frequency domain, thus facilitating the analysis of deformations. For each grid, the initial phase is extracted from the reference image, and the deformed phase is extracted from the deformed image. The phase difference between these two states is calculated for each direction, providing a measure of the displacements along the X and Y axes. These phase differences are then converted into displacements using the relation :

$$u_{(x,y)} = \frac{\Delta\phi_{(x,y)}}{2\pi k_{(x,y)}} \qquad (4)$$

- $\Delta\phi$: the phase difference
- k : the corresponding spatial frequency.

The displacement fields obtained are used to create displacement and strain maps, allowing a detailed visualization of the sample's deformations.

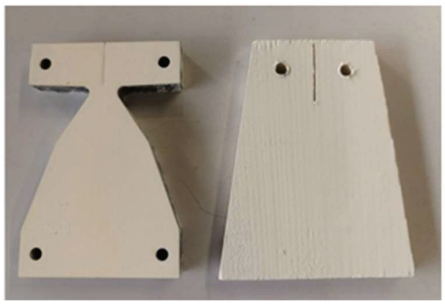

Figure 3 : Painting on the specimens

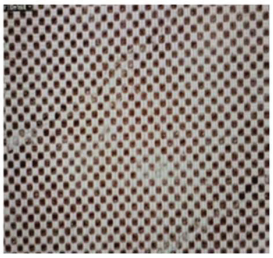

Figure 4 : Appearance of checkerboard

3 – EXPERIMENTAL PROTOCOL

To carry out the tests, a steel Arcan system was used for the MMCG specimens. Figure 5 illustrates the characteristics and geometry of this device. The design of the Arcan system features a central opening, allowing the checkerboard pattern engraved on the specimens to be visible during the tests [8].

This feature facilitates the observation and analysis of the periodic patterns required for the LSA method.

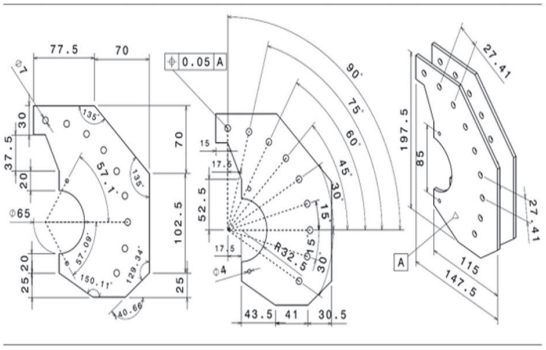

Figure 5 : Arcan Sytem

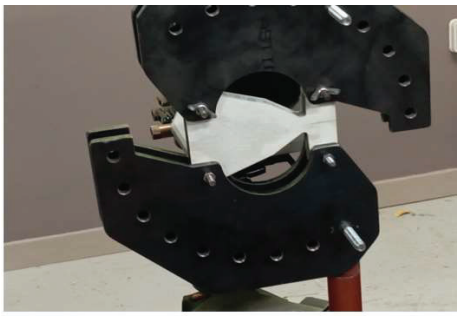

Figure 6 : Setting up the MMCG specimen

Due to its various loading angles, the Arcan system is versatile and suitable for all types of loading conditions, including mixed loading. It has been specifically designed to be compatible with CTS and MMCG specimens.

To conduct the tests, a Zwick/Roel tensile-compression machine with a loading capacity of 200 kN and equipped with a 50 kN force sensor was used. Two cameras mounted on tripods on each side of the specimen captured images of the checkerboard during the tests. Projectors were positioned to enhance the lighting on the specimen's surfaces to ensure high-quality images.

Figure 7 illustrates the entire experimental setup. It shows the steel Arcan system used to load the specimens. Imposed displacements control the movable grip of the testing machine (upper grip) at a speed of 0.005 mm/s and is equipped with a force sensor, ensuring precise control of the applied load.

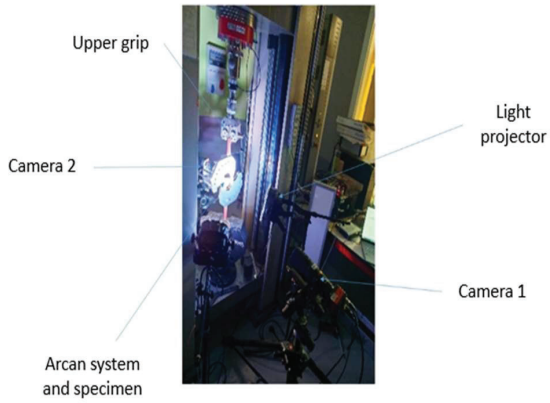

Figure 7 : Experimental setup

4 – RESULTS

In this section, we will analyze the results obtained after the tests. We will begin by visually observing the crack propagation direction.

4.1 CRACK PROPAGATION DIRECTION

After the tests, the first results observed visually are the crack propagation directions in each specimen. crack propagation always occurs along the direction of the fibers, as seen in the case of a large fiber angle (Figure 8).

This corresponds to the image taken at the 700th second, i.e., image 700 of specimen M23-a.

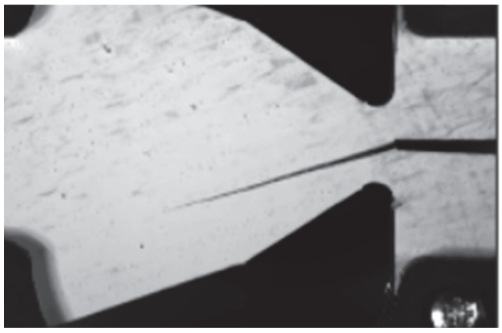

Figure 8 : Specimen M23-a, after the crack at t = 700s

4.2 DISPLACEMENT AND STRAIN MAP

Figures 9 (a) and (b) show a typical vertical displacement and the strain maps obtained using the LSA method applied to a MMCG specimen for 0% fiber angles. This displacement map allows us to measure the crack opening during the tests, while the strain map helps precisely determine the crack tip's position, representing the crack advancement.

https://doi.org/10.52202/080513-0203

The crack opening Uy is determined from the displacement maps following these steps :

- Two points, A and B, are chosen on each side of the crack lips, ensuring they are sufficiently far from the crack to avoid their displacement being influenced by local effects caused by the crack.
- The crack opening is calculated by measuring the difference in vertical displacement between points A and B.

The crack length is detected using the strain map, and then an image processing technique is applied in Python to determine the crack tip, as shown in Figure 10.

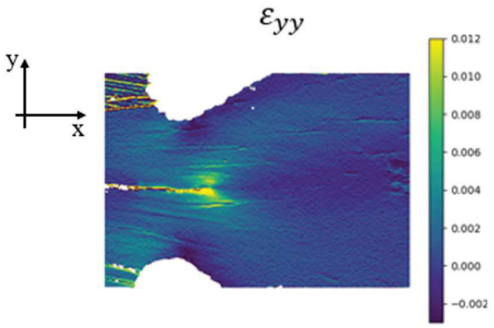

(a)

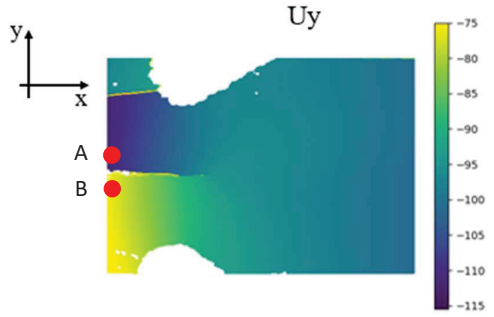

(b)

Figure 9 : (a) Vertical strain maps; (b) Vertical displacement maps

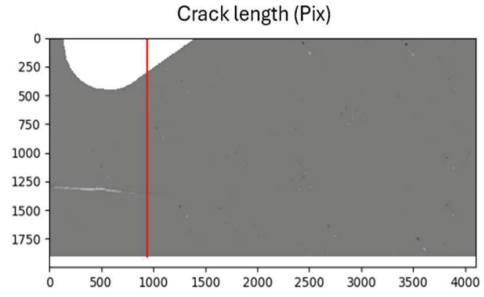

Figure 10 : Crack length

4.3 FORCE-OPENING CURVE

The force versus crack opening curves for two types of MMCG specimens are presented in Figure 11. despite the low number of repetitions, force peaks are higher with 0° fiber slope (graph a), compared to those with 23° fiber slope (graph b). Repeatability is quite good according to anatomy: M0-a and M0-b specimens are provided from the same beam, different from the M0-c one. M23 specimens from a to c are also from the same beam.

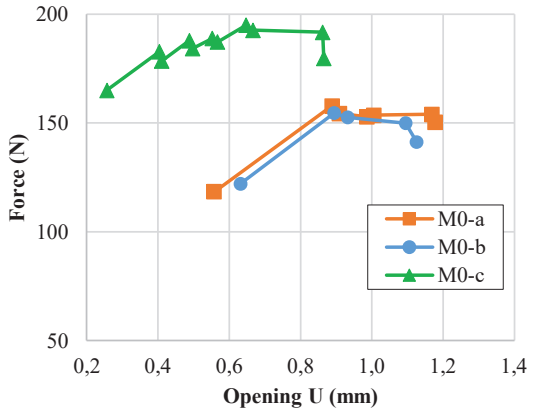

(a)

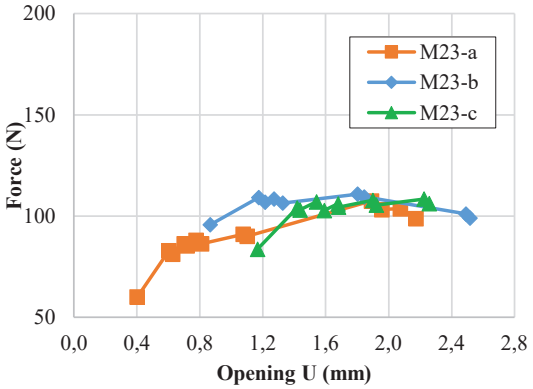

(b)

Figure 11 : (a) MMCG with 0° fiber slope; (b) MMCG with 23° fiber slope

4.4 ENERGY RESTITUTION RATE

The Figure 12 represents Gc, energy restitution rate, as a function of the crack length on the CAM2 side, i.e., the small checkerboard, calculated using the compliance method for MMCG specimens. For 0° specimens, the difference between M0-c and others illustrate the effect of anatomy on this value. Results for 23° show quite similar Gc values.

https://doi.org/10.52202/080513-0203

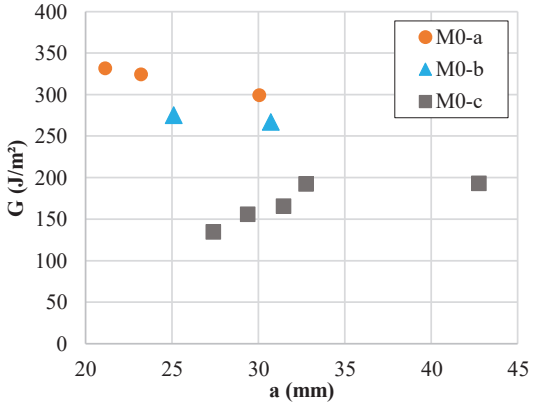

(a)

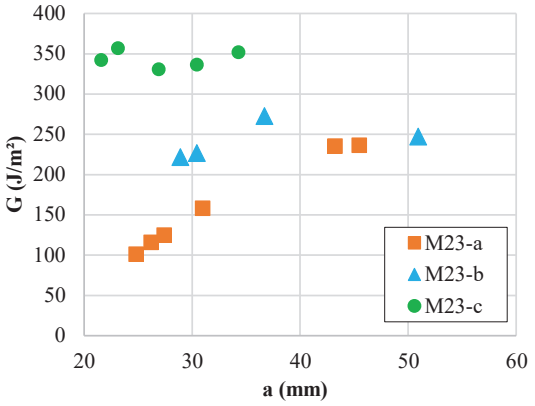

(b)

Figure 12 : Energy restitution rate as a function of crack length : (a) MMCG (0°) ; (b) MMCG (23°)

Table 1 summarizes mean values. The mean GCmax value appears to be independent of the sample geometry and grain slope. The opening mode based on perpendicular tensile strength predominates over the effect of shear induced by the grain angle.

Table 1 : Results of the energy release rate for all specimens

Code	Angle	Gc max (J/m²)	Standard deviation	Δa max (mm)
T0-a	0°	286	99	7,7
T0-b	**0°**			
M0-a	0°	267	70	12,1
M0-b	0°			
M0-c	0°			
M23-a	23°	288	62	6,5
M23-b	23°			
M23-c	23°			

4.5 DIFFERENCE BETWEEN CAMERAS

The energy restitution rate is calculated on both faces of the specimen, with Cam1 corresponding to the face with the large checkerboard and Cam2 corresponding to the face with the small checkerboard. Here are the G curves obtained for some specimens (figure 13).

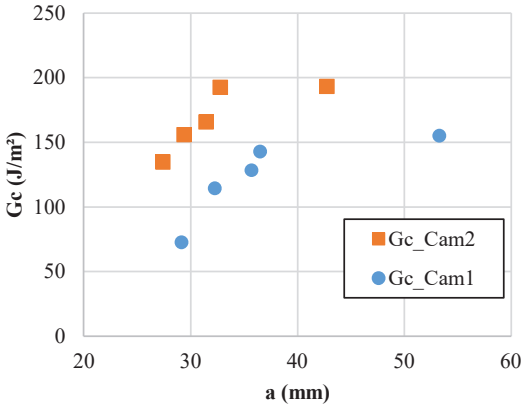

(a)

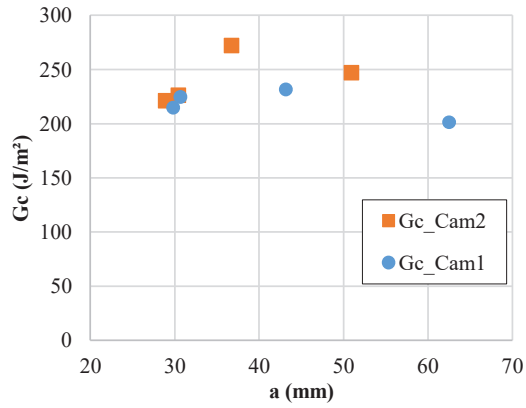

(b)

Figure 13 : Comparison of Gc between the two faces of the specimens (a) M0-c ; (b) M23-b

Due to its inherent heterogeneity, crack propagation in wood on the two faces is not synchronized. Cam 1 (large checkerboard) gives us higher values for the crack length, which is observed for all specimens (Blue points in Figure 13a,b).

5 – SCANNING ELECTRON MICROSCOPE (SEM) OBSERVATION

The objective is to track the crack progression through the tracheids and determine whether it propagates by fiber overlap. This involves understanding how cracks form and propagate in the fir wood. The hypothesis of fiber overlap remains to be verified using the Scanning Electron Microscope, as illustrated in Figure 14.

https://doi.org/10.52202/080513-0203

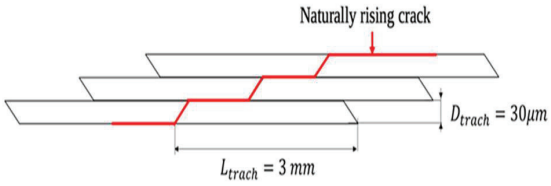

Figure 14 : Crack propagation through tracheid overlap.

To prepare samples for Scanning Electron Microscope (SEM) tests, the cracked side of the specimen was cut into a 1mm thick, 2mm wide, and 10mm long strip in the direction of crack propagation (Figure 15).

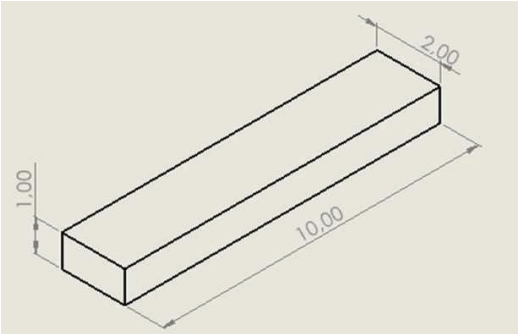

Figure 15 : Sample dimensions for SEM analysis for specimen M23-a

The tracheids are well-aligned, forming a regular network. In the images, the crack propagation is from right to left, Figure 16. This image shows a tracheid measuring approximately 1.075 mm in length.

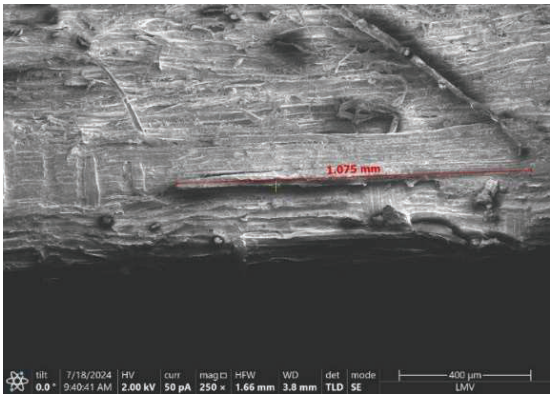

Figure 16 : Length of a tracheid (x 250)

The tracheid is visible along its entire length, and its elongated, tubular structure is clearly identifiable. This measurement falls between 0.5 to 4 mm, corresponding to the typical size of tracheids in softwood.

In Figure 17, two ligneous rays perpendicular to the tracheids appear, in which areolated spots are clearly visible. The intersections demonstrate how the tracheids are organized and interrupted regularly along the wood rays. The measured distance between two tracheid intersections is 469.4µm.

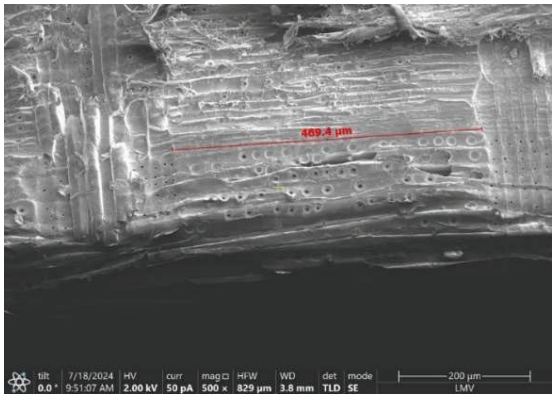

Figure 17 : Distance between two intersections (x 500)

Figure 18 illustrates the junction of a tracheid and a ligneous ray. On this cracked surface, the walls of the tracheids are cut in two, and they are partially separated from each other. This process ends in a junction with a ligneous ray. The presence density of ligneous ray could be an anatomical parameter influencing crack resistance.

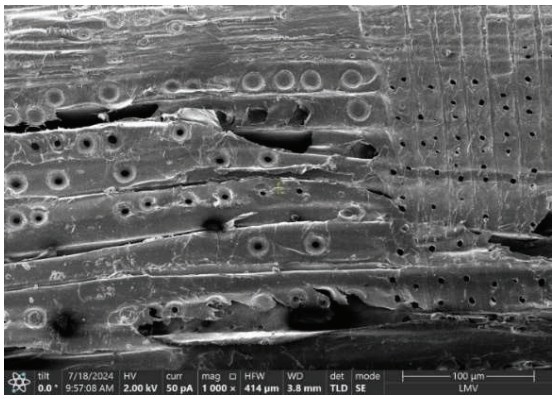

Figure 18 : After an intersection, a defibrated tracheid (x 1000)

6 – CONCLUSION

This work explored crack propagation in fir wood, considering the fiber orientation. This study developed two types of specimens: the TDCB (Tapered Double Cantilever Beam) specimen and the MMCG (Mixed Mode Crack Growth) specimen. The use of the MMCG specimen was due to the instability of the crack encountered in the TDCB specimen. A series of experimental tests were conducted using the Localized Spectral Analysis (LSA) technique, a non-contact field measurement method that allowed us to determine the crack opening and the crack advancement throughout the test. These are two important parameters for calculating the energy restitution rate.

https://doi.org/10.52202/080513-0203

The results show that the fiber angle has no significant impact on the trajectory and stability of cracks. Samples exhibit identical critical energy restitution rates according to their geometry and grain angle. Furthermore, although the hypothesis of fiber overlap was explored, Scanning Electron Microscope (SEM) observations showed uncertain results. Based on the weak and fragile behaviour in perpendicular tension, it can be concluded that wood's opening mode is predominant.

7 – ACKNOWLEDGMENTS

The authors wish to express their gratitude to the Polytech School of the University of Clermont Auvergne for the smooth progress of this work.

8 – REFERENCES

[1] FCLP, «Initiative pour rendre la construction plus écologique grâce au bois durable.,» 6 Decembre 2023. [En ligne]. Available: https://www.leboisinternational.com/. [Accès le 2024].

[2] P. Triboulot, P. Jodin, G. Pluvinage, "Mesure des facteurs d'intensité de contrainte critiques et des taux de restitution d'énergie dans le bois sur éprouvettes entaillées.", vol. Vol. 39, Ann. Sci. Forest, 1982.

[3] A. Bontemps, «Comportement mécanique des éléments de structure en bois de sapin pectiné soumis à un environnement variable.,» *Université Clermont Auvergne ,* n° %12023UCFA0016, pp. 100-150, 05 Juillet 2023.

[4] M. MEITE, «Characterization of cracking parameters by coupling image correlation and finite elements.,» *University of Limoges,* pp. 65-68, 15 June 2012.

[5] R. MOUTOU PITTI, «Découplage des modes mixtes de rupture dans les matériaux viscoélastiques orthotropes : modélisation et expérimentation,» *Université de Limoges,* n° %1472008, pp. 100-104, 15 Octobre 2008.

[6] M. Grédiac, B. Blaysat et F. Sur, «Extracting Displacement and Strain Fields from Checkerboard Images with the Localized Spectrum Analysis,» *SIGMA. Institut Pascal, UMR CNRS 6602, Université Clermont Auvergne. BP 10448,,* pp. 2-12, 8 Octobre 2018.

[7] M. Grédiac, B. Blaysat et F. Sur, A critical comparaison of some metrological parameters characterizing local digital image correlation and grid method., Experimental Mechanics, 2017, pp. 1-33.

[8] B. ODOUNGA, «Etude de la fissuration des bois tropicaux pa mesures des champs,» *Université Clermont Auvergne,* pp. 100-125, 14 Novembre 2018.

https://doi.org/10.52202/080513-0203